Journal of Groundwater Science and Engineering 14(2026) 252–270

Journal homepage: http://gwse.iheg.org.cn

Research Article

Hazard driven debris flow simulation and risk evaluation in the Karakorum Mountain ranges, Northern Pakistan

Nisar Ali Shah[1,2*], Muhammad Shafique[1,2], Benazeer Iqbal[1], Muhammad Ishfaq[3], Tanveer Ahmed[1], Israr Ullah[4]

[1] *GIS and Space Application in Geosciences (GSAG) Lab*, *National Center of GIS and Space Application (NCGSA)*, *Islamabad* 44000, *Pakistan*, *National Centre of Excellence in Geology*, *University of Peshawar*, *Peshawar* 25130, *Pakistan*.
[2] *National Centre of Excellence in Geology*, *University of Peshawar*, *Peshawar* 25130, *Pakistan*.
[3] *Abteilung Strukturgeologie und Geothermik*, *Universität Göttingen*, *Goettingen* 37077, *Germany*.
[4] *National Centre of Excellence in Geology*, *University of Peshawar*, *Peshawar* 25130, *Pakistan*.

Abstract: Northern Pakistan is highly susceptible to debris flows due to its complex geomorphic structure, steep topography, climate change, glaciation, monsoonal rainfall, active seismicity, deforestation, and human activities. Despite this, high-resolution, quantitative assessments of debris flow hazards are limited, constraining effective disaster risk management. This study aims to model a representative debris flow event in the Ghizer District to predict potential deposition areas and support emergency preparedness and sustainable land-use planning in this hazard-prone region. High-resolution Unmanned Aerial Vehicle (UAV)-derived topographic data were integrated with the Rapid Mass Movement Simulation (RAMMS-DF) model to simulate debris flow runout for three release scenarios, representing distinct and combined initiation zones. Satellite images and field validation were used to delineate release and erosion zones, while vulnerability and risk were assessed by mapping exposed elements including 210 buildings and a population of 1,500 and applying spatial multi-criteria analysis within a Geographic Information System (GIS) framework. The numerical simulation for the most critical event, Scenario 3 (representing simultaneous dual-source initiation), yielded the highest magnitude results with a total flow volume of 193,717 m^3, a peak flow height of 12.96 m, and a maximum impact pressure of 992.28 kPa. Vulnerability mapping identified infrastructure and agricultural land as the most exposed. Risk assessment showed that the combined scenario posed the greatest threat to local assets and communities. The study demonstrates that debris flow dynamics in high-mountain environments are non-linearly sensitive to initial release volumes and the interaction between multiple flow sources. Topographic controls such as channel confinement and slope variations are the primary drivers of flow intensity and energy dissipation. This research establishes a replicable, data-driven framework for quantitative risk assessment in data-limited mountainous regions. The resulting high-resolution hazard and risk maps provide a scientific basis for defining land-use restrictions, prioritizing slope stabilization, and guiding the placement of emergency infrastructure to support disaster-resilient development in northern Pakistan.

Keywords: Debris flow; Runout simulation; GIS; Vulnerability

Received: 20 Nov 2024/ Accepted: 13 Jan 2026/ Published: 30 Apr 2026

Introduction

Debris flows with high velocity and long runouts pose a significant threat to communities and infrastructure in mountainous regions (Abraham et al. 2021). Regions with rough topography, active erosion, and rainy seasons are susceptible to debris flows and are often triggered by prolonged and intense rainfall, floods, glacier melting, and glacial lake outbursts floods (Rybchenko et al. 2018).

*Corresponding author: Nisar Ali Shah, *E-mail address*: geologist.nisar07@gmail.com

DOI: 10.26599/JGSE.2026.9280082

Shah NA, Shafique M, Iqbal B, et al. 2026. Hazard driven debris flow simulation and risk evaluation in the Karakorum Mountain ranges, Northern Pakistan. Journal of Groundwater Science and Engineering, 14(2): 252-270.

2305-7068/© 2026 Journal of Groundwater Science and Engineering Editorial Office This is an open access article under the CC BY-NC-ND license (http://creativecommons.org/licenses/by-nc-nd/4.0)

Projected changes in mean and extreme temperatures, along with variations in precipitation patterns, are anticipated to significantly impact the frequency and magnitude of mass movements, such as landslides, debris flows, and avalanches, in mountainous environments (Knight, 2022; Eckert et al. 2024). These climate-driven changes are expected to exacerbate the risk of mass movements, posing challenges for hazard management and infrastructure in mountainous regions (Yamanoshita, 2019; Khan et al. 2022; Shahzad et al. 2024). Climate change-induced global warming and increasing precipitation in the mountainous ranges of the Himalayas, Karakorum and Hindukush, have increased the frequency of the debris flows (Dash et al. 2021; Sattar et al. 2022; Li et al. 2023). Moreover, the increase in population and associated infrastructure development, and expansion of hill roads on unstable slopes are destabilizing the natural ecosystem and triggering soil erosion and weathering that eventually activate landslides and debris flows during the rainy season, intensifying exposure, vulnerability and risk. Therefore, understanding and evaluating the debris flow-induced hazard, vulnerability and risk assessment from regional to local scales is critical for effective disaster mitigation, preparedness, adaptation, and land use planning (Zhou et al. 2022).

Evaluating and managing debris flow hazards pose a significant challenge for global disaster reduction efforts in mountainous regions. The data and techniques required for debris flow hazard and risk assessment are determined by the geographical scale, process mechanism, and potential risk to communities and infrastructure. Debris flow hazard assessment at a regional scale is often achieved through statistical analysis, hydrodynamic approaches, empirical methods, numerical methods, aerial photograph or satellite image interpretation, and Geographic Information System (GIS)-based morphometric analysis and geotechnical approaches, however, these methods have limited application for local-scale disaster management (Dash et al. 2021; Hou et al. 2021; Qiao et al. 2023). Debris flow assessment at a local scale mainly concentrates on site-specific conditions and is typically based on a precise evaluation of potential damages (Zou et al. 2016). It requires detailed analysis and relatively highly accurate data for selected indicators and models, and may serve as a basis for local disaster risk management, planning of technical mitigation projects, and land-use planning activities (Holub et al. 2012; Rajaneesh et al. 2025).

For debris flow hazard assessment at a local scale, various models have been developed and utilized across the globe, including the Flood and Debris Flow Simulation Model (FLO-2D), Dynamic Analysis of Landslides in Three Dimensions (DAN3D), Rapid Mass Movement Simulation - Debris Flow (RAMMS-DF), and Mass Flow Debris Mode Mdflow (Scheuner et al. 2011; Zhou et al. 2022; Cabral et al. 2023; Islam and Chattoraj, 2023; Ahmad et al. 2025). These models often evaluate the velocity, volume, depth, and runout distance, along with assessing the potential impacts on downstream land use, infrastructure, and communities. These models commonly utilize parameters including hydrological, release area, friction, stream morphology, meteorological and topographic parameters, and their accuracy depends on the quality of the input parameters and the resolution of the topographic parameters (Martini et al. 2023).

The Rapid Mass Movement Simulation (RAMMS) was originally designed to simulate snow avalanche and subsequently adapted to estimate the intensity and runout of debris flow and rock fall (Christen et al. 2010; Gan and Zhang, 2019). Prediction of debris flow is often difficult due to insufficient data and understanding of the triggering mechanisms, mainly rainfall and subsurface dynamics (Cai et al. 2025). However, back-analysis of past debris flow events can be effectively used to model potential future events in the future and associated risks (Simoni et al. 2012; Mikoš and Bezak, 2021; Turbessi et al. 2025).

Risk assessment of individual debris flow events at a local scale involves understanding the specific factors that contribute to the occurrence and impact of these events within a particular area. Researchers have investigated a range of methodologies and frameworks specifically designed for this scale to enhance the evaluation and mitigation of risks. Tang et al. (2022) applied an estimation-based semi-quantitative approach utilizing field data and hazard intensity to assess the vulnerability and risk levels of debris flows in specific rainfall scenarios at a local scale. Xiao et al. (2024) evaluated debris flow risk by integrating dynamic process-based hazard analysis with quantitative hazard zoning and the vulnerability of elements at risk, emphasizing both numerical simulation and spatial risk mapping. Based on the findings of the hazards associated with debris flows and the vulnerability of elements at risk, Chen et al. (2025) developed risk classification and mapping frameworks that integrate hazard intensity with vulnerability indicators to categorize debris-flow risk into multiple

levels for improved mitigation planning. Additionally, some researchers have examined the behavioral attributes of debris flows following significant seismic events by selecting watersheds distinguished by prevalent debris flow occurrences to investigate the implications for risk factors (Chen et al. 2024; Utley et al. 2025). The existing methodologies for assessing debris flow risk exhibit considerable divergence in analytical depth and resultant numerical outcomes, predominantly emphasizing macroscopic perspectives or qualitative characterizations. Consequently, the development of a quantitative framework aimed at evaluating debris flow risks at a local scale is critical (Gu et al. 2025). Therefore, developing a robust, data-driven approach to quantify debris flow risk at a local scale is crucial for improving disaster preparedness and risk management strategies.

Northern Pakistan, with its rugged topography, active seismicity, and fragile geology, is highly vulnerable to multiple natural hazards, including earthquakes, landslides, floods, debris flows, and Glacial Lake Outburst Floods (GLOFs). Additionally, the region is among the most climate-sensitive areas globally, experiencing rising temperatures and shifting precipitation patterns that have intensified extreme events such as debris flows and GLOFs in recent years. Previous studies have analyzed debris flows at a regional scale in northern Pakistan (Khan et al. 2013; Qing et al. 2020; Ali et al. 2021). However, their implementation at the local scale for hazard assessment, mitigation, and risk reduction remains limited, which is crucial for conducting accurate hazard and risk assessments. Despite limited advancements in understanding and modeling debris flow dynamics in recent years by (Ullah et al. 2024; Ahmad et al. 2025; Khan et al. 2025), a significant research gap remains concerning the local simulation of debris flow runout and associated risk in northern Pakistan. This study focuses on conducting a detailed local-scale debris flow hazard assessment in the Ghizer region of northern Pakistan using the RAMMS-DF model to simulate potential debris flow events and evaluate their impacts on downstream infrastructure and settlements under multiple scenarios. Unlike previous studies that often rely on empirical methods or single hazard scenarios, this research evaluates multiple release scenarios to identify critical risk conditions. To enhance risk assessment accuracy, we develop a comprehensive geospatial database of elements at risk by integrating high-resolution remote sensing data with field surveys. The study aims to provide spatially explicit insights that can guide land-use regulation, settlement planning, and the design of disaster prevention infrastructure in hazard-prone areas such as Khalti Village. By linking high-resolution debris flow modelling with vulnerability analysis, this research contributes to a more effective disaster risk management framework that informs evidence-based policy and sustainable land-use planning in the northern mountainous regions of Pakistan.

1 Study area

The study area is located in the Kohistan Island arc and Karakorum block, characterized by rough terrain, steep to gentle slopes, active denudation, glaciation, climatic conditions, and anthropogenic activities that favor widespread landslides, rock falls, scree slopes, and debris flows (Shafique et al. 2016; Shah et al. 2025). Ghizer District exhibits a rugged and steeply sloping topography, with elevations ranging from 1,632 m to 6,610 m above sea level. The terrain is dominated by deeply incised river valleys, extensive scree slopes, and unconsolidated Quaternary deposits that contribute to slope instability. Steep slopes, reaching inclinations of up to 83°, promote rapid sediment transport, particularly during intense precipitation events. The presence of debris fans at stream outlets further influences sediment deposition patterns, creating a dynamic geomorphic setting that enhances debris flow susceptibility (Shah et al. 2025). This complex topography, combined with active fluvial and mass movement processes, makes the region highly vulnerable to natural hazards such as landslides and debris flows. Geologically, the region lies within the tectonic framework of the Kohistan Island Arc and the Karakoram Block, separated by the Main Karakoram Thrust. The lithological units consist of the Kohistan Batholiths, Chalt Volcanic Group, Greenstone Complex, Darkot Group, Yasin Group, and Quaternary deposits, which include alluvial, colluvial, and lacustrine sediments (Searle, 2011; Ahmad et al. 2025). Glacial retreat, permafrost degradation, and intense precipitation, combined with unconsolidated sediments in steep, narrow catchments, enhance sediment mobilization and increase debris flow activity (Shah et al. 2025). The mean rainfall in Ghizer ranges from 1,002 mm/year to 2,873 mm/year (Shah et al. 2023).

The watershed selected for the study is located in Khalti village of Ghizer District, northern Pakistan, which is frequently exposed to debris flows (Fig. 1). However, the watershed lacks a debris flow monitoring system, and therefore the

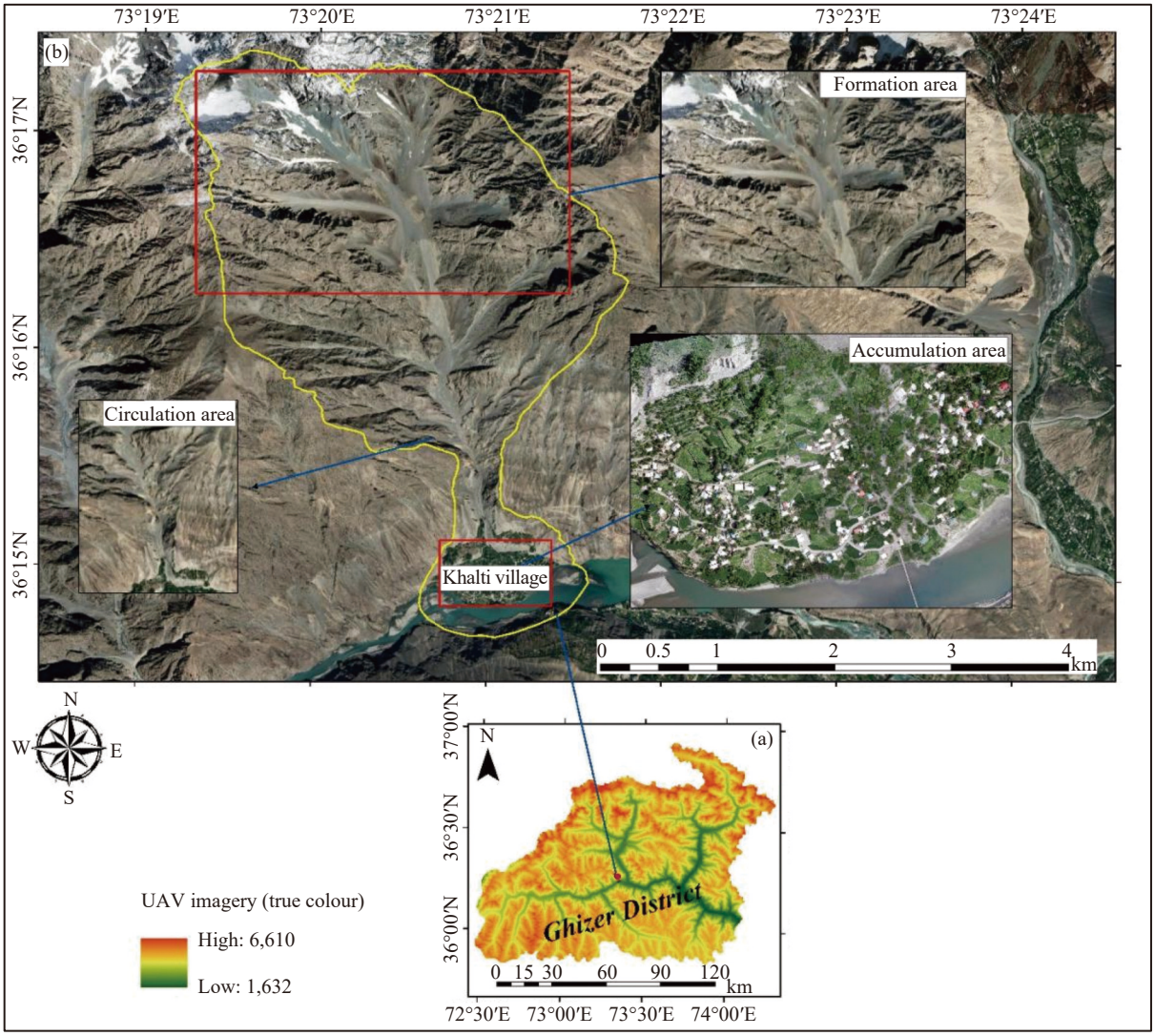

Fig. 1 Location map of the selected watershed (Khalti Village) for the debris flow modelling

Notes: (a) Elevation of the district, (b) Khalti catchment with streams, and the inset shows a zoomed-in view of UAV imagery of the fan

required data for simulating the debris flow were generated through field visits, satellite images, and interviews with local people. In July 1980, due to a major debris flow, a lake named Khalti was formed (Fig. 2), which still exists and provides scenic beauty for the area. Mainly triggered by intense precipitation, the debris flow damaged Khalti Village, including orchards and agricultural land. The watershed has recently experienced debris flows in the monsoon seasons (July – August) of 2010 and 2022, destroying agricultural land of the alluvial fan.

Fig. 2 Field photo of the Khalti Lake formed in 1980 due to a debris flow

The catchment has abundant loose material for debris flow and has the potential to damage the downstream infrastructure, agricultural land, and communities on both sides of the stream. The density of loose boulders increases from the base to the apex point of debris, mostly on the scree slope (Fig. 3). The size of these boulders ranges from 2 feet to 5 feet. The streams in the catchment are perennial. Both sides of the catchment are covered by cliff faces. The approximate distance between the cliff faces is approximately 350 m. Highly metamorphic rocks, including marble and schist, were observed. The moraine deposits have angular shapes. The approximate height of the

Fig. 3 Field photographs showing the nature of the material and erosion in the catchment

cross-section is 240 m. The thickness of the loose material is approximately 12–15 m.

2 Material and methods

Unmanned Armed Vehicle (UAV) DJI Inspire 2 was used to collect very high-resolution topographic information and aerial photos of the area. Extensive fieldwork was carried out to acquire UAV data to study the characteristics of the debris flow event area and to validation of the elements-at-risk data (houses, roads, agricultural land, forest, and bridge data). UAV data were processed using Pix4D software. Pix4D processing involves five major steps, i.e., pre-processing, point cloud generation, mesh generation, Digital Surface Model (DSM) computation, and orthomosaic generation. The spatial resolution of the DSM and orthomosaic imagery generated through Pix4D was 0.2 m and 0.04 m, respectively. This data were resampled to a spatial resolution of 2 m for the processing of the Digital Elevation Model (DEM) in RAMM-DF software.

It was difficult to acquire the UAV data for the high elevated portion of the basin due to rough terrain features and strong wind effects. Hence, for the elevated areas, the Advanced Land Observing Satellite Phased Array Type L-band Synthetic Aperture Radar (ALOS PALSAR) DEM was used with the spatial resolution of 12.5 m to extract the topographic information and was resampled to 2 m. ArcGIS and very high-resolution UAV imagery were utilized for mapping the elements at risk, including buildings, roads, agricultural land, orchards, and lakes. These elements-at-risk data were validated in the field; moreover, the population of the Khalti village was also recorded in the field. The methodology adopted for the study has two important steps: i) DEM Analysis, and ii) numerical modelling in RAMM-DF software.

2.1 RAMM-DF software for debris flow simulation

RAMMS employs the depth-averaged shallow water equations for granular flow in a single-phase model (Mikoš and Bezak, 2021) and delivers accurate predictions of flow heights, velocities, runout distances, and flow paths of debris flow in natural three-dimensional terrain (Simoni et al. 2012). It generally uses the Voellmy-Salm fluid flow continuum model, which is based on the Voellmy friction model (Salm, 1993; Mikoš and Bezak, 2021). It utilizes the Voellmy fluid friction model, which divides the friction resistance into i) dry coulomb-type friction resistance denoted by Mu (μ) and ii) viscous-turbulent friction Xi (ξ). The aforementioned parameters are often calibrated; however, additional parameters, including the stop parameters and the simulation resolution, might also have an impact on the modelling results (Bezak et al. 2019; Mikoš and Bezak, 2021). The parameters μ and ξ are also called the coefficient of friction and coefficient of turbulence, respectively (Hussin et al. 2012). The simplified representation of total frictional resistance (S) is represented by equation 1:

$$S = \mu \cdot \rho \cdot H \cdot g \cdot \cos(\varnothing) + (\rho g u^2)/\xi \qquad (1)$$

Where: ρ indicates the density, g denotes the gravitational acceleration, $\varnothing$ is the slope angle, H is the mean height of the debris flow and indicates the flow velocity. Furthermore, the flow behavior is determined by the friction coefficient μ, whereas the turbulent coefficient is responsible for a faster-moving flow (Bartelt et al. 2015; Qodri et al. 2021). The methodology flowchart for the proposed study is shown in Fig. 4.

2.2 Parameters, calibration, and validation of RAMMS-DF

For performing numerical simulation, three parameters need to be specified: (1) the digital elevation model (DEM); (2) the predefined release area; and (3) friction parameters (μ and ξ) (Christen et al. 2010; Fan and Galoie, 2025). These parameters for RAMMS are selected based on topography, release area, hydrograph, release volume, and friction characteristics. The major step involved in the RAMMS simulation starts with the topographic data. Scheuner et al. (2011); Krishnapriya et al. (2024) proposed that scenario-based runout simulation is critical for obtaining reliable results for sediment deposition and accumulation.

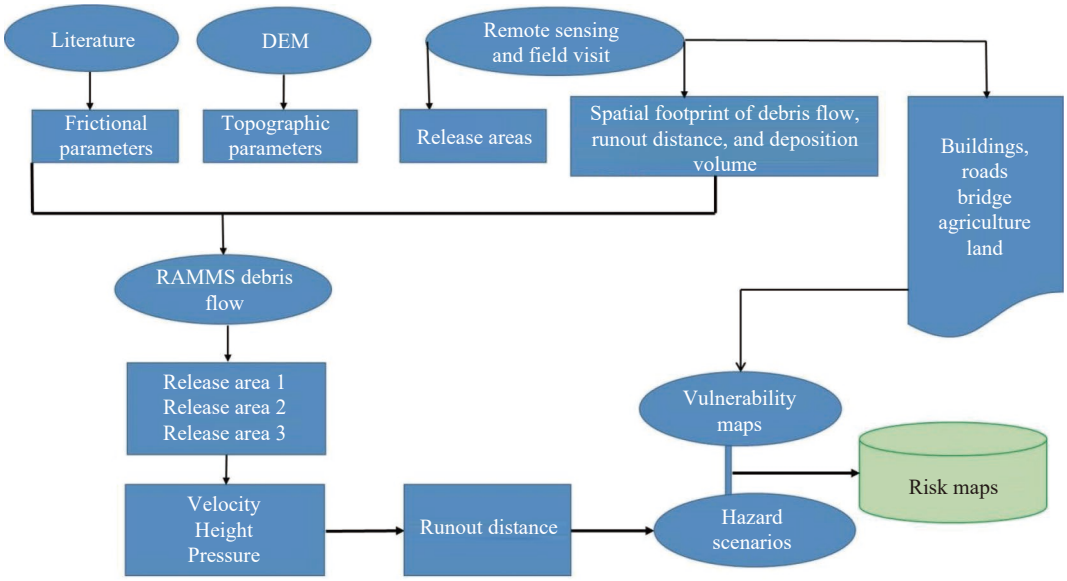

Fig. 4 Flowchart of the methods for the hazard scenarios, vulnerability and risk assessments of all scenarios for debris flow

Due to the absence of direct field monitoring for debris flow parameters such as volume, velocity, and depth, model calibration was performed using back-analysis. Field-mapped runout distances and deposition depths were used to iteratively adjust RAMMS-DF parameters to best replicate observed flow behavior. The release area (61,784.4 m^2 with an estimated depth of 1 m) was delineated through satellite image interpretation and field validation. Initial parameterization involved adjusting the dry Coulomb friction coefficient (μ) and the turbulent flow coefficient (ξ). The optimal match with the observed runout was obtained using a friction coefficient (μ) of 0.07 and a turbulent coefficient (ξ) of 550 m/s^2 (Table 1), which provided the best alignment with field data. Model sensitivity to these parameters was assessed by examining their influence on runout distance, deposition pattern, and channel conformity (Fig. 5).

In this study, simulations were performed for three scenarios considering two probable release areas with different initial volumes for the first and second scenarios, while the third scenario was based on the combined release area of the first and second release areas (Fig. 6). These parameters were carefully selected based on the topographic profile, hydrological characteristics, release volume, and material properties to ensure a realistic simulation of debris flow behavior. The DEM provides the fundamental terrain framework, while

Table 1 Parameters for RAMMS-DF software in scenario-based analysis following (Gardezi et al. 2021)

Analysis	Friction Coefficient, μ	Turbulent coefficient, ξ (m/s^2)	DEM (m)
Scenario-1	0.07	550	2
Scenario-2	0.07	550	2
Scenario-3	0.07	550	2

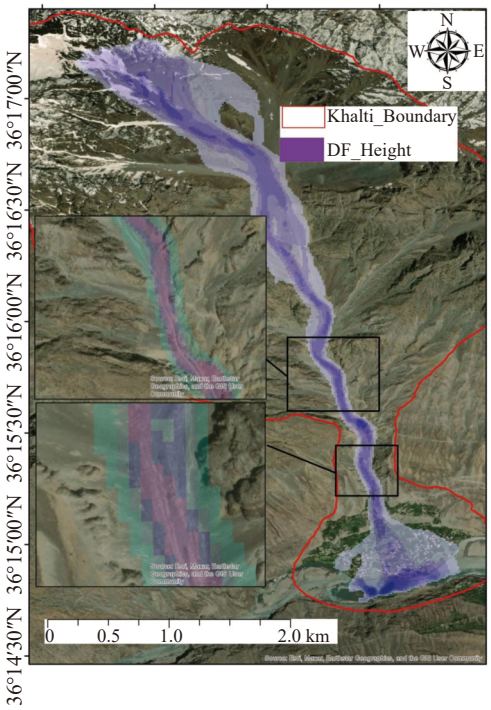

Fig. 5 Simulated debris flow height using RAMMS-DF for the calibrated values (μ = 0.07, and ξ = 550 m/s^2), showing the simulation

Notes: The purple gradient represents the modeled debris flow height (DF_Height) along the flow path. The insets highlight key deposition zones for calibration and validation.

the release areas are delineated using remote sensing and field data. The friction parameters were calibrated iteratively to match observed runout distances, ensuring that the model accurately represents real-world debris flow dynamics. The erosion areas were also identified from the UAV data and field observations, and both release and erosion areas were then imported into the RAMMS software for generating scenarios of slope failures in the upstream.

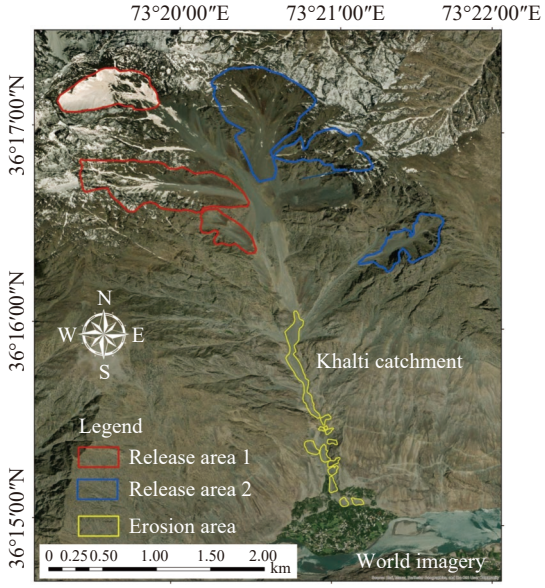

Fig. 6 Release areas and erosion material for debris flow

Notes: Red colored polygons indicate release area 1, blue colored polygons indicate release area 2, and yellow-colored polygons show the erosion area.

Although the input parameters remain consistent across all scenarios, variations in spatial distribution and initiation dynamics significantly influence hazard and risk levels. Scenario 3, representing the simultaneous activation of both release areas, results in greater flow volume, velocity, and impact pressure, leading to the highest risk. This study employs high-resolution UAV-derived topographic data and RAMMS modeling, ensuring accurate debris flow simulation. Model calibration accounts for entrainment, deposition, and energy dissipation, aligning results with observed geomorphological features. The integrated hazard and risk maps validate Scenario 3 as the most critical, emphasizing the need to consider multi-source initiation in risk assessments. After generating all three scenarios in RAMMS, the obtained data was exported to ArcGIS for the debris flow hazard mapping and combinations of debris flow velocities and depths were identified and classified into distinct zones of hazard (Table 2).

Table 2 Values used for hazard assessment zoning following (Tang et al. 1993)

S. No	Debris flow hazard zoning	Flow velocity (m/s)	Flow height (m)
01.	Extremely high-hazard area	> 5	> 3
02.	High hazard area	2–5	1–3
03.	Medium hazard area	1–2	0.5–1
04.	Low hazard area	< 1	< 0.5

2.3 Vulnerability assessment

For vulnerability assessment, the elements at risk data in the alluvial fan were digitized in ArcGIS using UAV imagery. The selected elements at risk include infrastructure, including houses, roads, bridges, agricultural land, and orchards. The majority of the population depends on agricultural land for their livelihood. Hence, the elements-at-risk data utilized for vulnerability assessments consider the socio-economic factors, environmental factors, and physical indicators. For vulnerability assessment, the Analytic Hierarchy Process (AHP) technique was used to determine the weight of each factor that evaluates the vulnerability of the selected elements at risk to the debris flow (Cao et al. 2017; Shah et al. 2023; Li et al. 2024). AHP is a robust, structured, and widely recognized decision-making framework that breaks down the elements into multiple levels and provides both qualitative and quantitative analysis (Xiao et al. 2020), and is particularly suited for vulnerability assessments in complex environments. AHP effectively integrates subjective expert assessments with objective field data by adopting a systematic pairwise comparison approach. This procedure ensures logical prioritization of criteria by quantifying expert knowledge into a consistent numerical scale (Saaty, 2008). The weights assigned to the evaluation factors are based on a literature review, expert opinion, and field observations (Table 3).

Table 3 Shows assigned weights to elements at risk for vulnerability assessment based on AHP

Element at risk	Assigned weights
Buildings	0.40
Roads	0.25
Agriculture land	0.15
Orchards	0.06
Bridge	0.10
Lake	0.04

2.4 Risk assessment

Risk refers to the possibility of injuries or losses that occur as a result of a hazard. Risk assessment involves the investigation of both hazards and vulnerabilities (Alcántara-Ayala and Sassa, 2023), The United Nations Department of Humanitarian Affairs (1992) quantified risk by employing hazard and vulnerability. Risk maps are computed by integrating vulnerability maps with hazard maps following the equation proposed by Ouyang et al. (2019) and Zhou et al. (2022).

$$\text{Risk} = \text{Hazard} \times \text{Vulnerability} \quad (2)$$

3 Results

3.1 Hazard assessment

RAMMS–DF provided quantitative data on debris flow runout distance, flow height, pressure, and flow velocity along the flow path (Dash et al. 2021). In Scenario 1, initiated from a single release area, the maximum flow height reached 10.21 m in the transportation zone (Fig. 7), with a peak impact pressure of 771.27 kPa, indicating destructive potential for downstream infrastructure. The flow attained a maximum velocity of 19.64 m/s near the source due to steep slopes and confined channels. Fig. 8a depicts the early-stage dynamics of the debris flow at the source area, where the flow attained a maximum velocity due to steep slopes and channel confinement, leading to initial entrainment of material. Downslope, the debris mass entrained a gross volume of 19,747 m^3 of material through basal and lateral erosion. Due to simultaneous sediment deposition along the channel path, the net volume at the alluvial fan increased from 78,769 m^3 to 97,338 m^3 (Fig. 8b), reflecting a total volume gain of 18,569 m^3.

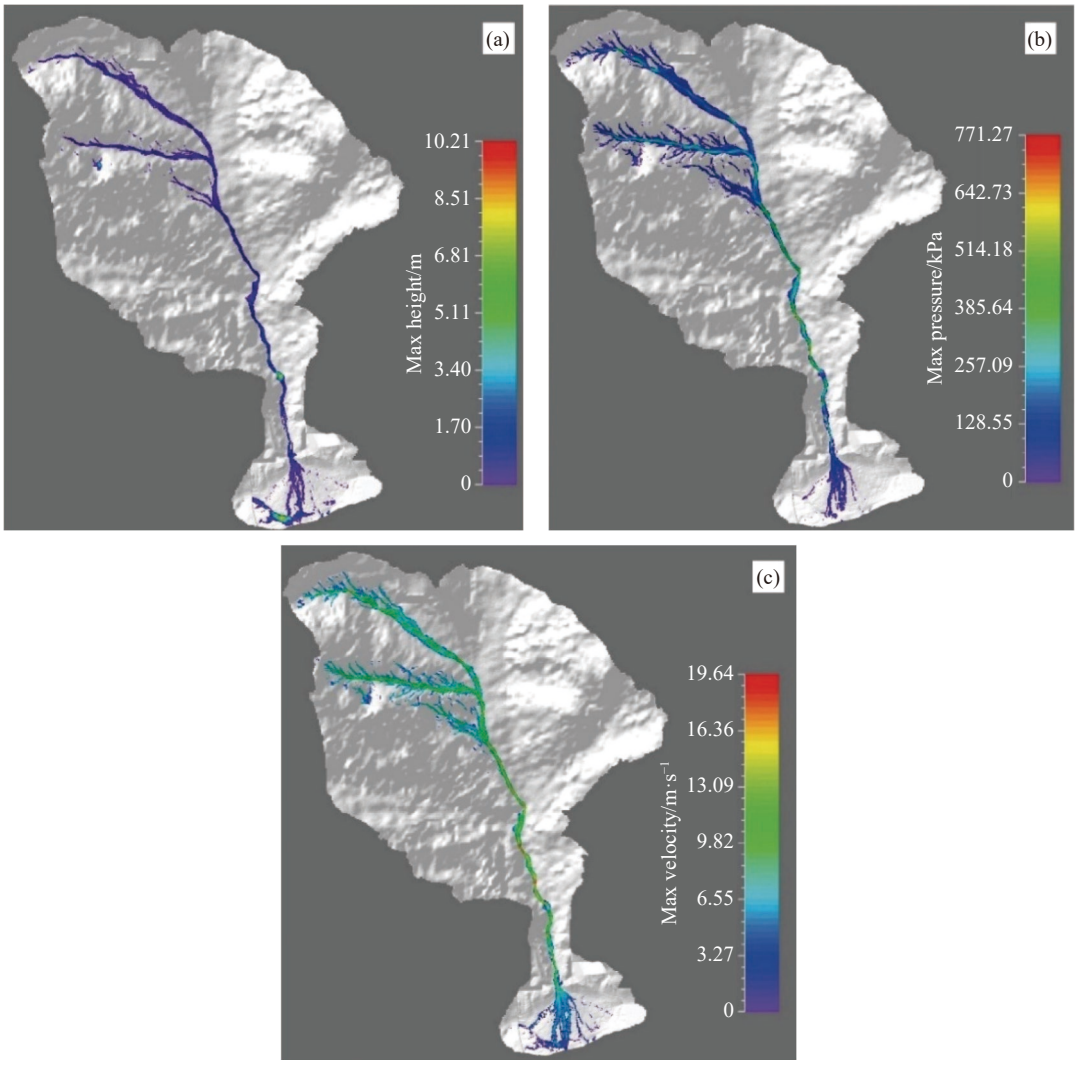

Fig. 7 Simulation output from the source zone to the depositional zone for Scenario 1: (a) height, (b) pressure, and c) velocity

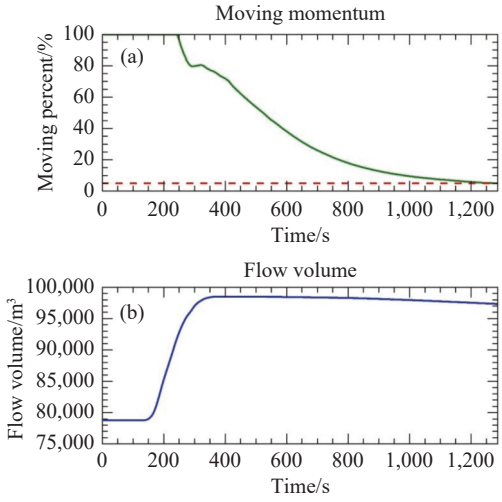

Fig. 8 Debris flow dynamics over time for Scenario 1

Notes: (a) Shows the moving percent (green line, left Y-axis), which indicates the percentage of total debris mass in motion, and moving momentum (red dashed line), which reflects the energy of the moving flow. (b) Shows the flow volume (blue line, Y-axis). The x-axis in both figures represents time

Scenario 2 represents a more energetic debris flow event compared to Scenario 1. The simulation indicates a peak flow height of 11.08 m, an impact pressure of 1,012.53 kPa, and a high erosive and destructive potential due to increased momentum and sediment fluid interaction. The simulation indicates a maximum velocity of 22.50 m/s (Fig. 9). Fig. 10a illustrates the initial stages of the debris flow near the source area. Along its downslope trajectory, the flow entrained an additional 25,917 m^3 of material, increasing the total volume from an initial 89,986 m^3 to 115,903 m^3 (Fig. 10b). The flow culminated in a final deposition thickness of 10.08 m, highlighting its increased transport efficiency and spatial impact relative to Scenario 1.

Scenario 3 simulates the most critical and complex event, characterized by the simultaneous failure of both identified release areas. The debris flow reached a maximum flow height of 12.96 m and attained a peak impact pressure of 992.28 kPa, reflecting a highly energetic and destructive flow. The maximum velocity was 22.27 m/s (Fig. 11, Table 4), indicating significant flow bulking and vertical material accumulation. Although Scenario 3 generated the largest flow volume and height, its peak velocity and pressure were slightly lower than those of Scenario 2. This difference reflects topographic controls: The larger volume in Scenario 3 caused greater thickness and lateral spreading,

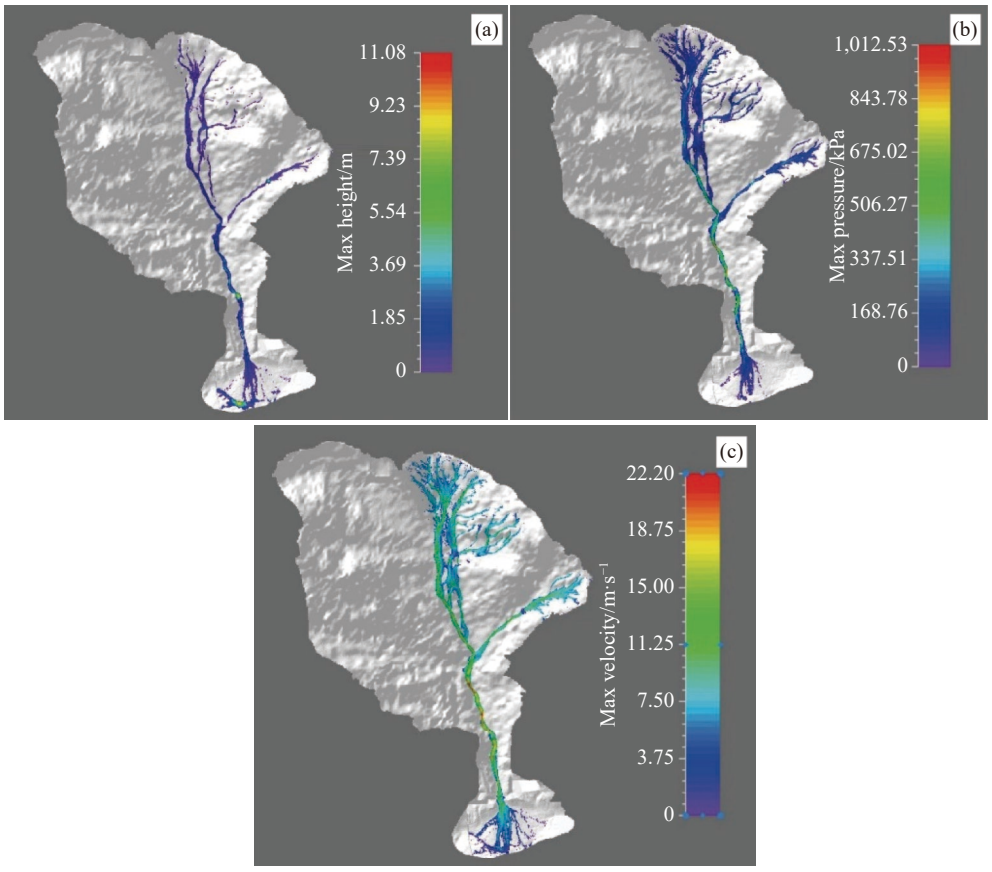

Fig. 9 Simulation output from the source zone to the depositional zone for Scenario 2: (a) height, (b) pressure, and (c) velocity

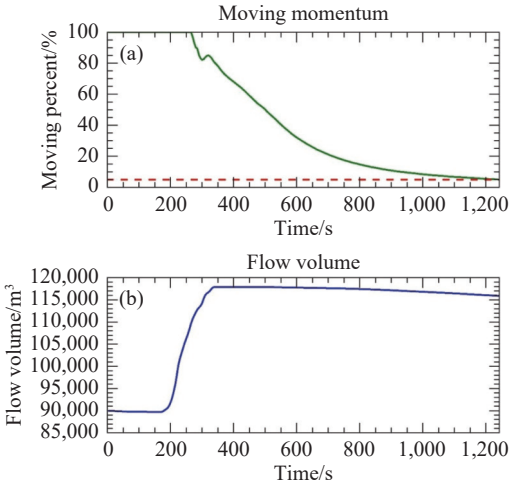

Fig. 10 Debris flow dynamics over time for Scenario 2

Notes: (a) Shows the moving percent (green line, left Y-axis), which indicates the percentage of total debris mass in motion, and moving momentum (red dashed line), which reflects the energy of the moving flow. (b) Shows the flow volume (blue line, y-axis). The x-axis in both figures represents time

dispersing energy and increasing frictional resistance, whereas the confined channel in Scenario 2 concentrated momentum, yielding higher local velocity and pressure despite the smaller volume. These observations are directly supported by RAMMS-computed results, which quantitatively account for topographic and hydraulic factors, ensuring a physically consistent, model-based interpretation rather than a purely qualitative explanation.

Fig. 12a illustrates the initial stages of the debris flow near the source area, where the combined release volume was 168,709 m^3. As the flow advanced, it entrained a gross volume of 28,713 m^3 of material from the identified erosion zones. Accounting for internal depositional processes along the transport channel, the net volume at the final depositional area increased to 193,717 m^3 (Fig. 12b), reflecting a total volume gain of 25,008 m^3 at the alluvial fan.

Hazard maps for the three simulated scenarios were developed using RAMMS–DF outputs, with classification based on debris flow velocity and depth thresholds (Table 2). Each map delineates four hazard zones: Low, medium, high, and very high (Fig. 13). Across all scenarios, debris flows

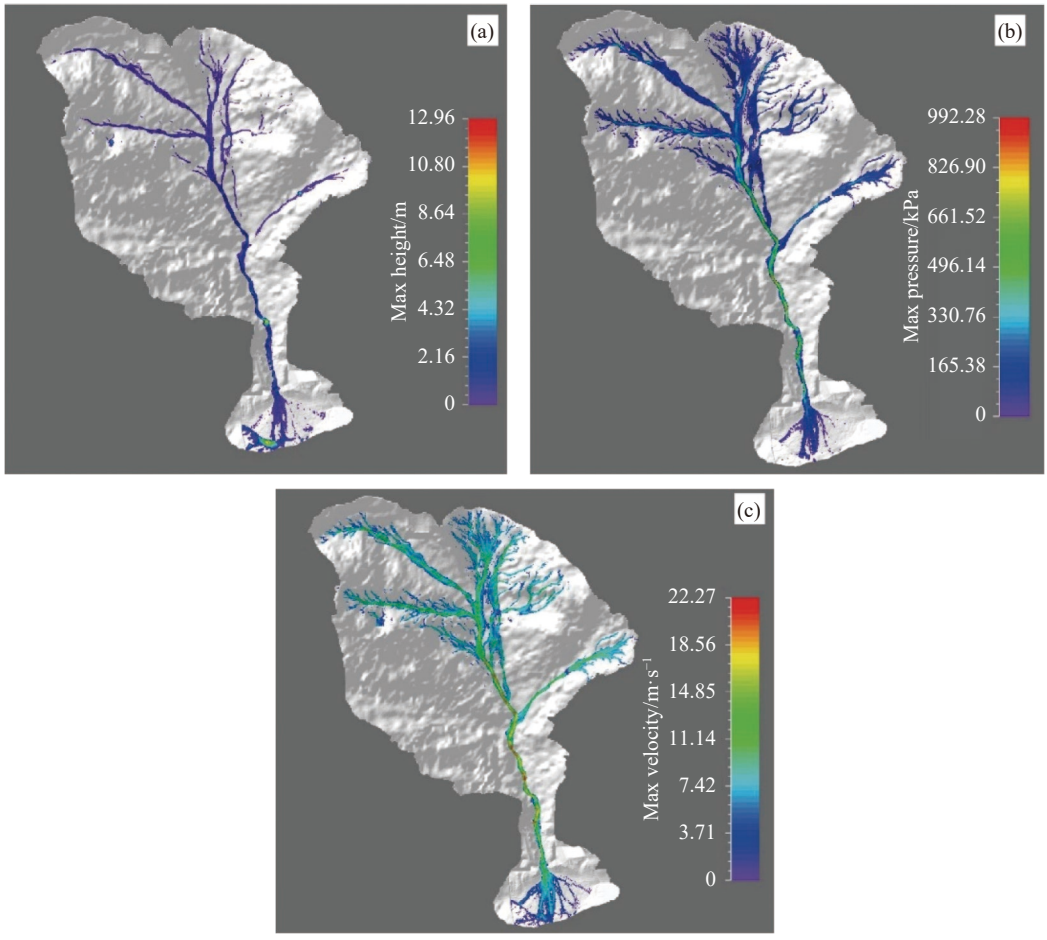

Fig. 11 Simulation output from the source zone to the depositional zone for Scenario 3: a) height, b) pressure, and c) velocity

Table 4 Summary of simulation output values

Scenario	Max Flow Height (m)	Peak Impact Pressure (kPa)	Max Velocity (m/s)
Scenario 1	10.21	771.27	19.64
Scenario 2	11.08	1012.53	22.50
Scenario 3	12.96	992.28	22.27

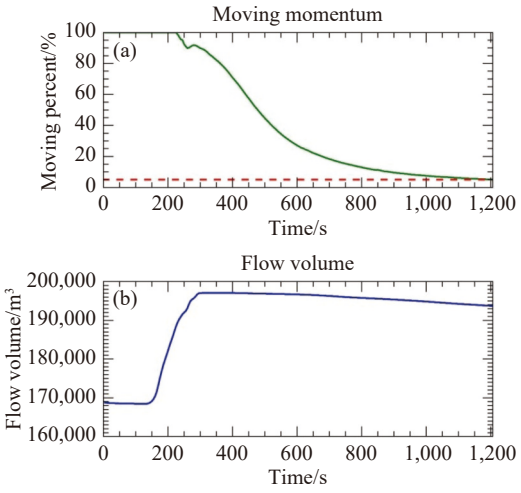

Fig. 12 Debris flow dynamics over time for Scenario 3

Notes: (a) Shows the moving percent (green line, left y-axis), which indicates the percentage of total debris mass in motion, and moving momentum (red dashed line), which reflects the energy of the moving flow. (b) Shows the flow volume (blue line, y-axis). The x-axis in both figures represents time

were primarily confined to steep channel gradients and deposited material within the alluvial fan. The flow paths consistently fell within high to very high hazard zones, indicating areas of intense energy, substantial flow depth, and sediment accumulation. These zones overlapped with critical elements at risk, including infrastructure and agricultural land. Scenario comparison shows that hazard intensity and spatial extent increase with flow volume and complexity. Scenario 1 presented localized high hazard near the depositional area. Scenario 2, with a larger release and more entrainment, expanded the high hazard coverage. Scenario 3, featuring dual-source initiation, produced the most extensive high and very high hazard zones, posing additional risk of river blockage and potential upstream flooding. The variability in hazard exposure is largely governed by terrain morphology, release volume, and proximity to main flow channels.

3.2 Vulnerability assessment

A comprehensive vulnerability assessment was conducted to evaluate the exposure of buildings, agricultural land, orchards, roads, and bridges to potential debris flow hazards. The assessment incorporated both physical and socio-economic dimensions, recognizing that infrastructure and land use patterns significantly influence disaster impacts at the local scale. Among these, building footprints serve as the primary vulnerability indicator, as they account for both social and physical dimensions of risk. The study identified 210 buildings, including 198 residential homes, 10 shops, one school, and one religious site, with a total population of 1,500.

Vulnerability maps were generated for all three simulated debris flow scenarios. The vulnerability classification was performed using the Natural Breaks (Jenks) method in ArcGIS, producing four classes: Low, moderate, high, and very high. These classes reflect increasing degrees of exposure and potential loss. Across all scenarios, vulnerability is negligible (0) in the upstream catchment due to the absence of built structures or critical infrastructure. However, vulnerability increases significantly in the alluvial fan area, where population centers and cultivated land are concentrated.

In Scenario 1, the debris flow originates from a single source with moderate flow intensity. The low vulnerability zone spans 1,377,100 m^2, while moderate, high, and very high vulnerability zones occupy 71,739 m^2, 6,498 m^2, and 486 m^2, respectively. The relatively small, high and very high vulnerability areas reflect the localized nature of this scenario and its limited runout extent.

In Scenario 2, a larger release volume and more aggressive flow dynamics increase exposure. The low vulnerability class extends over 1,702,140 m^2, while moderate, high, and very high classes cover 51,021 m^2, 37,152 m^2, and 3,141 m^2, respectively (Table 5). The considerable expansion of high and very high vulnerability areas signals a significant increase in infrastructure and agricultural risk, underscoring the need for more focused protective measures.

Scenario 3, simulating the simultaneous activation of both release areas, exhibits the highest spatial vulnerability. The low vulnerability zone increases to 2,818,670 m^2, while moderate, high, and very high zones span 42,255 m^2, 32,499 m^2, and 3,951 m^2, respectively. This scenario shows the greatest impact on infrastructure, with debris flow encroaching upon densely developed and economically valuable zones (Fig. 14). Additionally, the potential for river blockage introduces secondary flood hazards, further elevating the

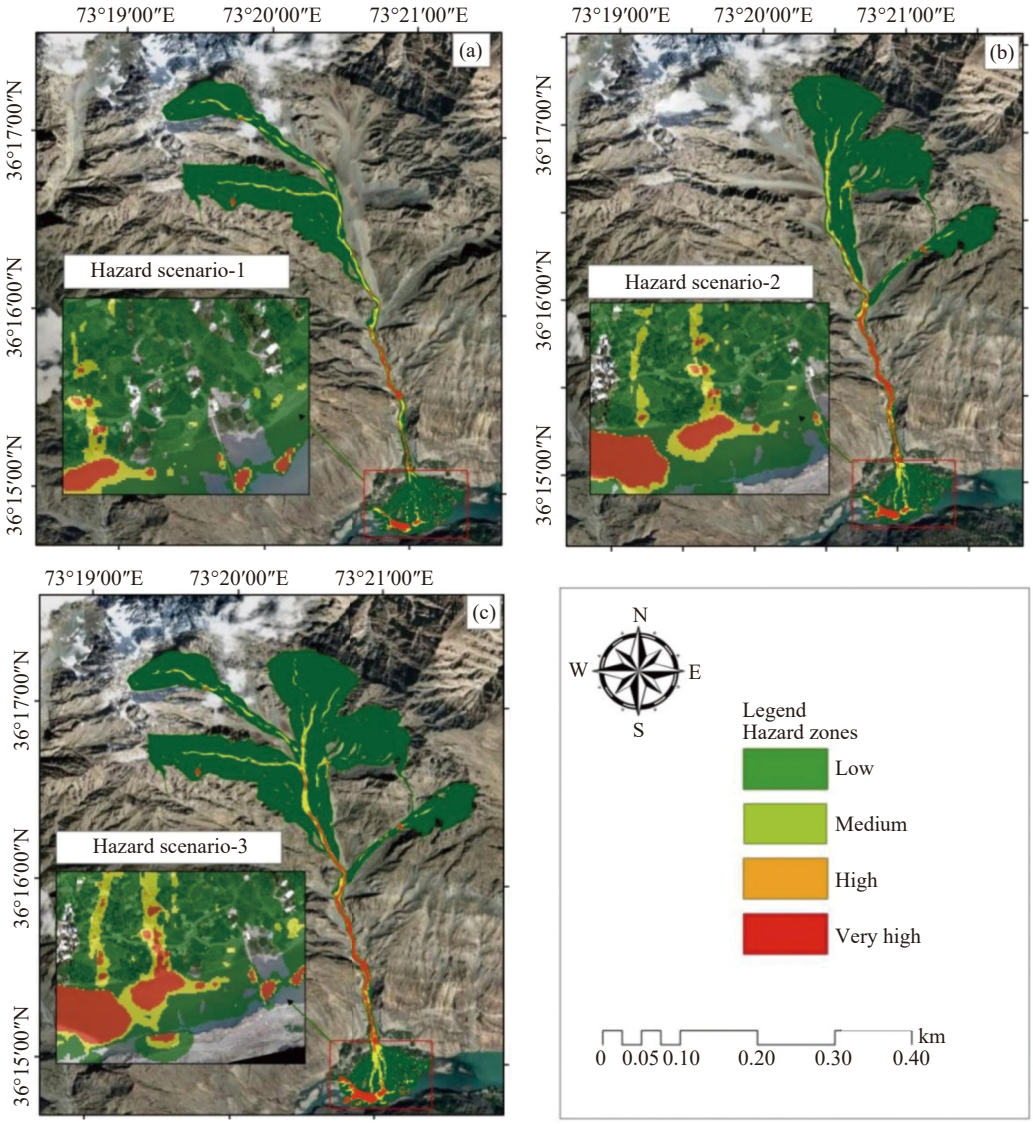

Fig. 13 Hazard maps of debris flow for all three scenarios based on height: (a) Scenario 1. (b) Scenario 2. (c) Scenario 3. The insets show zoomed-in views of low to very high hazard classes for each scenario

Table 5 Spatial distribution of vulnerability zones for each scenario

Scenario	Low vulnerability/m^2	Moderate vulnerability/m^2	High vulnerability/m^2	Very high vulnerability/m^2
Scenario 1	1,377,100	71,739	6,498	486
Scenario 2	1,702,140	51,021	37,152	3,141
Scenario 3	2,818,670	42,255	32,499	3,951

vulnerability of downstream communities and increasing the compound risk profile.

3.3 Risk assessment

The normalized hazard and vulnerability maps for all three scenarios were integrated to generate risk assessment maps, classifying the study area into four risk levels. A key aspect of the risk assessment is the human population and infrastructure exposed to debris flow hazards, particularly the number of potential fatalities or injuries. Table 6 presents the distribution of buildings and people across the different risk levels for each scenario.

In Scenario 1, the debris flow originates from a single release area, with a relatively lower flow volume and impact energy compared to the other scenarios. The risk assessment indicates that while agricultural land, roads, and some infrastructures are exposed, most elements at risk fall within the low to moderate risk categories. The Khalti bridge, a crucial infrastructure component, remains in the

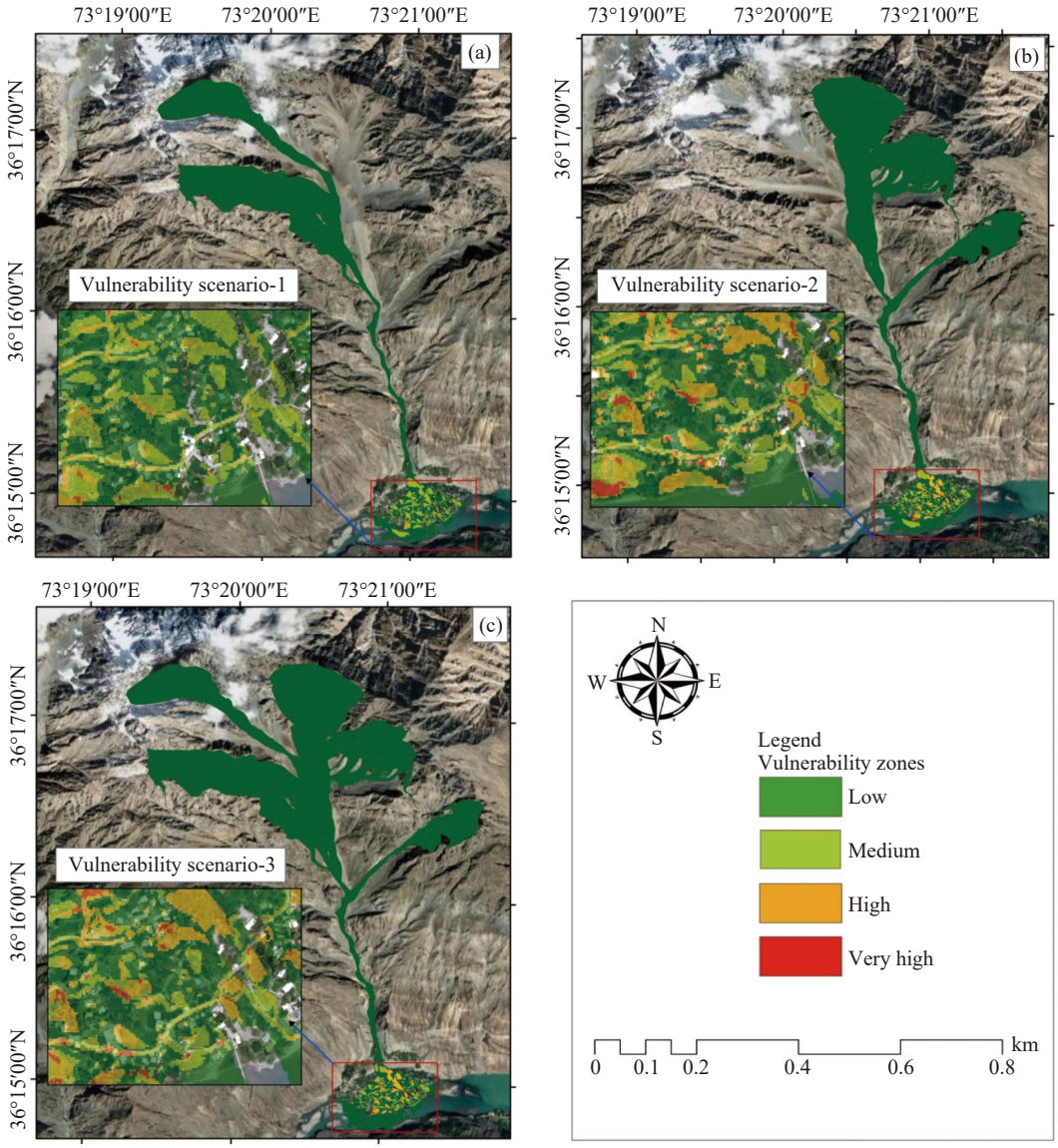

Fig. 14 Debris flow vulnerability maps for all three scenarios. (a) Scenario 1; (b) Scenario 2; (c) Scenario 3. The insets show zoomed-in views of low to very highly vulnerable zones for each class

Table 6 Shows the number of houses and persons in risk classes for all three scenarios

Scenarios	Low risk		Medium risk		High risk		Very high risk	
	Houses	Person	Houses	Person	Houses	Person	Houses	Person
1	165	1378	21	166	9	72	3	24
2	149	1192	32	248	12	96	5	40
3	134	1072	40	320	16	128	8	64

low-risk category due to limited flow intensity in its vicinity.

In Scenario 2, the debris flow volume increases due to a larger initial release and higher erosion along the flow path. This results in an expansion of high-risk zones, particularly affecting additional sections of roads and agricultural land. The maximum velocity and pressure exerted by the debris flow also increase, leading to greater infrastructure exposure. However, the Khalti bridge remains in the low-risk class, as the primary deposition zones do not significantly impact its structural integrity.

Scenario 3 represents the simultaneous activation of both release areas 1 and 2, leading to the highest total debris flow volume and a substantial increase in the affected area. This scenario exhibits the greatest impact, with extensive deposition zones, higher flow heights, and widespread infras-

tructure exposure. Notably, roads passing through the main depositional zones are categorized under high to very high risk, while agricultural land and orchards also experience significant risk levels. A critical observation in this scenario is that the Khalti bridge, which remained in the low-risk category in the first two scenarios, now has one end classified under medium risk. This is due to the potential for river blockage and increased water levels, which could pose secondary flood hazards to the nearby community.

Since Scenario 3 occurs concurrently with Scenarios 1 and 2, the integrated risk assessment reveals a compounding effect, where the total risk exposure surpasses that of individual scenarios. The combined hazard and risk maps highlight an expansion of high to very high-risk zones, demonstrating that the simultaneous occurrence of debris flows from both release areas significantly amplifies the overall impact on the study area (Fig. 15).

4 Discussion

4.1 Debris flow dynamics and hazard behavior

The simulation results reveal distinct spatial and temporal patterns of debris flow behavior across the modeled scenarios, governed by the interplay between release dynamics and terrain configuration. Debris flow mobility and hazard intensity were shown to be strongly influenced by catchment morphology, flow volume, and entrainment

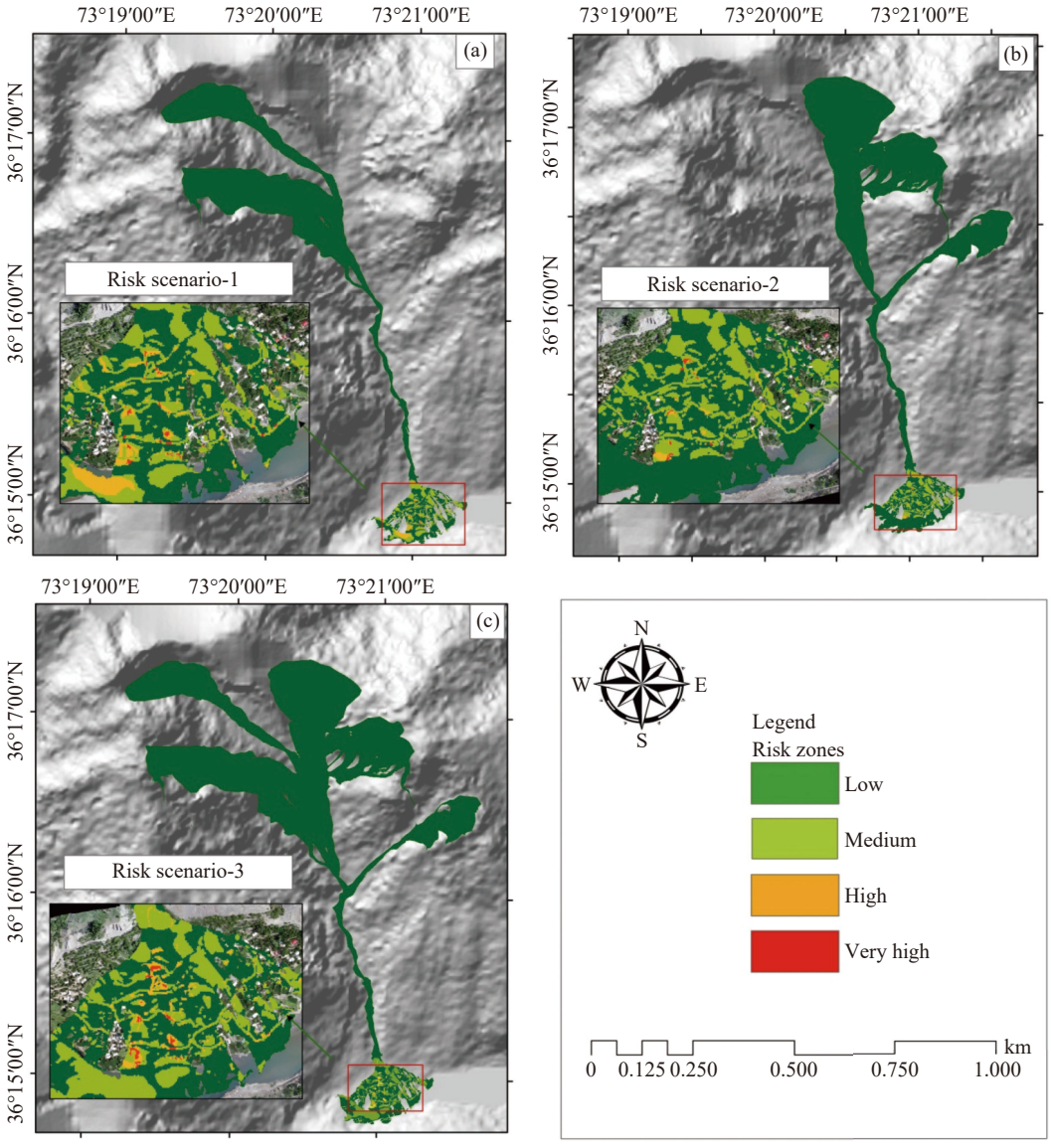

Fig. 15 Debris flow risk maps for all three scenarios: (a) Scenario 1, (b) Scenario 2, (c) Scenario 3, the insets show zoomed-in views of the risk maps

processes. Proximity to main channels and elevation relative to the flow path emerged as key determinants of impact severity. Although a geospatial database of exposed elements was utilized, its role was primarily to support and refine risk quantification rather than serve as an independent analytical focus. By applying physically based modeling in a data-scarce, high-mountain environment, this study contributes valuable insights for disaster risk management and highlights the necessity of integrating high-resolution simulations with field-based exposure mapping to support hazard monitoring, early warning systems, and climate adaptation planning.

The scenario-based approach proved effective in capturing spatial variability in debris flow behavior and provides a robust foundation for targeted hazard mitigation and land-use planning. The substantial increase in hazard severity under dual-source scenarios suggests that compound triggering events significantly alter flow momentum and deposition behavior, intensifying risk in downstream zones. This indicates that hazard assessments based on single-trigger assumptions may substantially underestimate impact potential in complex mountain environments. Moreover, the spatial correspondence between modeled flow paths and geomorphic controls such as slope breaks, channel narrowing, and depositional fan geometry reflects the dominant influence of topographic forcing in directing debris flow trajectories. This supports the notion that localized terrain configurations can either constrain or amplify flow energy, a factor that must be integrated into any predictive modeling framework. The successful reproduction of observed depositional patterns also highlights the value of high-resolution elevation models in accurately capturing micro-topographic features that govern flow spreading and sediment entrapment. These findings emphasize that realistic hazard mapping in high-relief, data-poor regions depends not only on robust physical modeling but also on precise topographic input and scenario-driven design.

4.2 Vulnerability and risk implications

The vulnerability and risk patterns revealed in this study underscore the compounding impact of flow volume and spatial dynamics on infrastructure exposure. The clear escalation of risk across scenarios demonstrates that vulnerability is not static but highly sensitive to debris flow behavior, particularly in geomorphologically active zones like alluvial fans. The integration of high-resolution topographic data with structured vulnerability weighting enabled a nuanced differentiation of exposure across the landscape, illustrating that even small shifts in flow trajectory can disproportionately affect critical infrastructure such as roads, bridges, and residential clusters. Importantly, the risk transition observed in key assets (e.g., settlements, the Khalti Bridge, and agricultural land) reflects how hazard evolution can alter system vulnerabilities under compound triggering conditions.

This dynamic interplay between flow mechanics and built environment distribution reinforces the need for scenario-based risk modeling to capture potential thresholds of system failure and cascading hazards, such as secondary flooding from channel blockages. By coupling AHP-driven vulnerability metrics with physics-based simulation outputs, this study moves beyond traditional qualitative assessments and offers a replicable, spatially explicit framework suitable for operational risk management in remote, data-poor settings. The findings highlight that accurate risk zoning depends not only on hazard magnitude but also on the alignment of exposure with flow-prone terrain features, a perspective often overlooked in coarser regional-scale models.

This refined approach supports the development of targeted, asset-specific mitigation plans and justifies the integration of high-resolution data into early warning systems and resilience planning in high mountain environments. The spatial distribution of high- and very high-risk zones identified in this study can serve as a practical reference for land-use and infrastructure planning in the Khalti watershed. Specifically, zones categorized as very high risk should be designated as non-developable or restricted construction areas, while high-risk zones may require slope stabilization, protective barriers, or engineered retaining structures to reduce hazard exposure. Moderate-risk zones could accommodate limited development following stringent engineering design codes and continuous monitoring. In addition, the modelled hazard pathways can guide the alignment of disaster prevention roads and evacuation routes, ensuring safe connectivity to low-risk areas during debris flow or secondary flood events. These spatial guidelines bridge the gap between hazard modelling and its application in community-level disaster preparedness and sustainable spatial planning.

4.3 Comparison with previous studies

Existing studies often emphasize the importance of

integrating advanced modeling techniques with comprehensive vulnerability assessments, yet many lack the application of high-resolution topographical data, such as that derived from UAV-based Digital Elevation Models (DEMs). Compared to previous regional-scale assessments that relied on empirical models or coarse DEMs (Melo et al. 2018; Dash et al. 2021; Ahmed et al. 2025), this study demonstrates that UAV-derived high-resolution DEMs significantly enhance the accuracy of hazard simulations. The combination of precise topographic inputs and advanced physics-based modeling bridges the gap between qualitative risk perception and quantitative disaster analysis, as also recommended by Zou et al. (2016) and Rajaneesh et al. (2025). Additionally, the use of AHP for vulnerability weighting allows a transparent, structured integration of both physical and socio-economic exposure factors, which is critical for multi-criteria risk evaluation (Saaty, 2008). By utilizing RAMMS-DF in a scenario-based framework, this study aligns with recent global findings that underscore the necessity for localized models to capture the variability and complexity of debris flow behavior in different geographical contexts. This approach is particularly valuable in developing countries where resource constraints often limit field-based vulnerability assessments.

4.4 Limitations and future directions

However, the study also acknowledges limitations. While RAMMS effectively simulates flow dynamics, it lacks the capability to model interactions between solid and fluid phases, which may affect deposition accuracy (Hussin et al. 2012; Fan and Galoie, 2025). Furthermore, the absence of long-term monitoring data restricts the calibration of model outputs against historical debris flow events. Although the model outputs align with field observations and past event indicators, additional validation using historical event reconstruction would further strengthen the reliability of the results. Future research should explore multi-phase modeling techniques and incorporate historical event calibration for improved simulation accuracy.

Conclusions

The study established a quantitative framework for debris flow risk assessment in the high-relief terrain of northern Pakistan by integrating UAV-derived topographic data with RAMMS-DF numerical modeling. The following conclusions are drawn from the analysis:

(1) **Non-linear Sensitivity of Flow Dynamics:** Debris flow behavior is highly sensitive to initial release volumes and the interaction between multiple source zones. Minor increases in sediment entrainment or the activation of secondary release areas result in non-linear increases in runout distance, flow depth, and impact pressure.

(2) **Topographic Controls on Hazard Intensity:** Local terrain morphology, specifically channel confinement and slope variation, is the primary driver of flow intensity. While larger volumes in Scenario 3 led to greater lateral spreading, the confined channel in Scenario 2 concentrated momentum, producing higher local velocities and impact pressures.

(3) **Sediment Budget and Erosion Patterns:** Erosion is most pronounced along the upper and middle reaches of the catchment, while deposition dominates the alluvial fan. The runout simulation for the most devastating event (Scenario 3) resulted in a maximum flow volume of 193,717 m^3 and a peak flow height of 12.96 m.

(4) **Spatial Dynamics of Vulnerability and Risk:** Vulnerability is spatially dynamic and governed by the alignment of infrastructure with flow paths. The combined scenario (Scenario 3) transitioned critical infrastructure, such as the Khalti Bridge, into higher risk categories due to potential channel blockage and secondary flooding.

(5) **Scientific Basis for Land-Use Planning:** The resulting high-resolution hazard and risk maps provide actionable insights for defining land-use restrictions and identifying safe zones for infrastructure. By delineating zones of varying hazard intensity, this study supports evidence-based decision-making for disaster-resilient development in data-limited mountainous regions

References

Abraham MT, Satyam N, Reddy SKP, et al. 2021. Runout modeling and calibration of friction parameters of Kurichermala debris flow, India. Landslides, 18: 737−754. DOI：10.1007/s10346-020-01540-1.

Ahmad N, Shafique M, Hussain ML, et al. 2025. Integrated debris flow hazard and risk assessment using UAV data and RAMMS, a case study in northern Pakistan. Natural Hazards, 121(2): 1463−1487. DOI：10.1007/s11069-024-06862-0.

Ahmad T, Jan MQ, Drüppel K. 2025. Geology of the central Kohistan Arc, Northern Swat,

Kalam (NW, Pakistan), results of a new 1: 50, 000 scale geological mapping. Journal of Maps, 21(1): 2572765. DOI：10.1080/17445647.2025.2572765.

Ahmed M, Titti G, Trevisani S, et al. 2025. Is higher resolution always better? A comparison of open-access DEMs for optimized slope unit delineation and regional landslide prediction. Natural Hazards and Earth System Sciences, 25(7): 2519−2539. DOI：10.5194/nhess-25-2519-2025.

Alcántara-Ayala I, Sassa K. 2023. Landslide risk management: From hazard to disaster risk reduction. Landslides, 20(10): 2031−2037. DOI：10.1007/s10346-023-02140-5.

Ali S, Haider R, Abbas W, et al. 2021. Empirical assessment of rockfall and debris flow risk along the Karakoram Highway, Pakistan. Natural Hazards, 106: 2437−2460. DOI：10.1007/s11069-021-04549-4.

Bartelt P, Bühler Y, Christen M, et al. 2015. RAMMS-DF User Manual. WSL Institute for Snow and Avalanche Research SLF, Davos, Birmensdorf, Switzerland. Available on http://ramms.slf.ch/ramms/, last access, 28.

Bezak N, Sodnik J, Mikoš M. 2019. Impact of a random sequence of debris flows on torrential fan formation. Geosciences, 9(2): 64. DOI：10.3390/geosciences9020064.

Cabral V, Reis F, Veloso V, et al. 2023. A multi-step hazard assessment for debris-flow prone areas influenced by hydroclimatic events. Engineering Geology, 313: 106961. DOI：10.1016/j.enggeo.2022.106961.

Cai S, Zhang Z, Yang X, et al. 2025. The modified theoretical model for debris flows predication with multiple rainfall characteristic parameters. Scientific Reports, 15(1): 12402. DOI：10.1038/s41598-024-84199-1.

Cao C, Xu P, Chen J, et al. 2017. Hazard assessment of debris-flow along the baicha river in Heshigten Banner, Inner Mongolia, China. International Journal of Environmental Research and Public Health, 14(1): 30. DOI：10.3390/ijerph14010030.

Chen M, Tang C, Xiong J, et al. 2024. Spatio-temporal mapping and long-term evolution of debris flow activity after a high magnitude earthquake. Catena, 236: 107716. DOI：10.1016/j.catena.2023.107716.

Chen TL, Wu YH, Chiu YH. 2025. Debris flow risk characteristics and potential spatial mitigation strategies under extreme rainfall events. Climate Services, 40: 100618. DOI：10.1016/j.cliser.2025.100618.

Christen M, Kowalski J, Bartelt P. 2010. RAMMS: Numerical simulation of dense snow avalanches in three-dimensional terrain. Cold Regions Science and Technology, 63(1): 1−14. DOI：10.1016/j.coldregions.2010.04.005.

Dash RK, Kanungo DP, Malet JP. 2021. Runout modelling and hazard assessment of Tangni debris flow in Garhwal Himalayas, India. Environmental Earth Sciences, 80: 1−19. DOI：10.1007/s12665-021-09637-z.

Eckert N, Corona C, Giacona F, et al. 2024. Climate change impacts on snow avalanche activity and related risks. Nature Reviews Earth and Environment, 5(5): 369−389. DOI：10.1038/s43017-024-00540-2.

Fan J, Galoie M. 2025. Assessment of physical parameters impacts on debris flow modeling with RAMMS. Scientific Reports, 15(1): 36393. DOI：10.1038/s41598-025-20303-3.

Gan J, Zhang YS. 2019. Numerical simulation of debris flow runout using Ramms: A case study of Luzhuang Gully in China. Computer Modeling in Engineering and Sciences, 981−1009. DOI：10.32604/cmes.2019.07337.

Gardezi H, Bilal M, Cheng Q, et al. 2021. A comparative analysis of attabad landslide on january 4, 2010, using two numerical models. Natural Hazards, 107: 519−538. DOI：10.1007/s11069-021-04593-0.

Gu Z, Yao X, Zhu X. 2025. Debris flow susceptibility in the Jinsha River Basin, China: a Bayesian assessment framework based on geomorphodynamic parameters. Natural Hazards and Earth System Sciences, 25(10): 3957−3975. DOI：10.5194/nhess-25-3957-2025.

Holub M, Suda J, Fuchs S. 2012. Mountain hazards: reducing vulnerability by adapted building design. Environmental Earth Sciences, 66: 1853−1870. DOI：10.1007/s12665-011-1410-4.

Hou S, Cao P, Li A, et al. 2021. In Debris flow hazard assessment of the Eryang River watershed based on numerical simulation. IOP Conference Series: Earth and Environmental Science. IOP Publishing: 062002. DOI：10.1088/1755-1315/861/6/062002.

Hussin H, Quan Luna B, Van Westen C, et al. 2012. Parameterization of a numerical 2-D debris flow model with entrainment: A case

study of the Faucon catchment, Southern French Alps. Natural Hazards and Earth System Sciences, 12(10): 3075−3090. DOI: 10.5194/nhess-12-3075-2012.

Islam MA, Chattoraj SL. 2023. Modelling landslides in the Lesser Himalaya region using geospatial and numerical simulation techniques. Arabian Journal of Geosciences, 16(8): 480. DOI: 10.1007/s12517-023-11541-8.

Khan MA, Haneef M, Khan AS, et al. 2013. Debris-flow hazards on tributary junction fans, Chitral, Hindu Kush Range, northern Pakistan. Journal of Asian Earth Sciences, 62: 720−733. DOI: 10.1016/j.jseaes.2012.11.025.

Khan MA, Mustaffa Z, Harahap ISH, et al. 2022. Assessment of physical vulnerability and uncertainties for debris flow hazard: A review concerning climate change. Land, 11(12): 2240. DOI: 10.3390/land11122240.

Khan MU, Tian S, Chen N, et al. 2025. Understanding the formation mechanism of rainfall and snowmelt jointly induced Bicharh Nallah debris flow, North Pakistan. Environmental Earth Sciences, 84(3): 86. DOI: 10.1007/s12665-024-12054-7.

Knight J. 2022. Scientists' warning of the impacts of climate change on mountains. PeerJ, 10: e14253. DOI: 10.7717/peerj.14253.

Krishnapriya V, Rajaneesh A, Sajinkumar K, et al. 2024. A rapid run-out assessment methodology for the 2024 Wayanad debris flow. Npj Natural Hazards, 1(1): 41. DOI: 10.1038/s44304-024-00044-5.

Li L, Lin H, Qiang Y, et al. 2024. A combination weighting method for debris flow risk assessment based on t-distribution and linear programming optimization algorithm. Plos one, 19(6): e0303698. DOI: 10.1371/journal.pone.0303698.

Li Y, Zou Q, Hao J, et al. 2023. Risk assessment of debris flows along the Karakoram Highway (Kashgar-Khunjerab Section) in the context of climate change. International Journal of Disaster Risk Science, 14(4): 586−599. DOI: 10.1007/s13753-023-00501-1.

Martini M, Baggio T, D'Agostino V. 2023. Comparison of two 2-D numerical models for snow avalanche simulation. Science of The Total Environment, 896: 165221. DOI: 10.1016/j.scitotenv.2023.165221.

Melo R, van Asch T, Zêzere JL. 2018. Debris flow run-out simulation and analysis using a dynamic model. Natural Hazards and Earth System Sciences, 18(2): 555−570. DOI: 10.5194/nhess-18-555-2018.

Mikoš M, Bezak N. 2021. Debris flow modelling using RAMMS model in the Alpine environment with focus on the model parameters and main characteristics. Frontiers in Earth Science, 8: 605061. DOI: 10.3389/feart.2020.605061.

Ouyang C, Wang Z, An H, et al. 2019. An example of a hazard and risk assessment for debris flows—A case study of Niwan Gully, Wudu, China. Engineering Geology, 263: 105351. DOI: 10.1016/j.enggeo.2019.105351.

Qiao Z, Li T, Simoni A, et al. 2023. Numerical modelling of an alpine debris flow by considering bed entrainment. Frontiers in Earth Science, 10: 1059525. DOI: 10.3389/feart.2022.1059525.

Qing F, Zhao Y, Meng X, et al. 2020. Application of machine learning to debris flow susceptibility mapping along the China–Pakistan Karakoram Highway. Remote Sensing, 12(18): 2933. DOI: 10.3390/rs12182933.

Qodri MF, Noviardi N, Mase LZ. 2021. Numerical modelling based on Digital Elevation Model (DEM) analysis of debris flow at Rinjani Volcano, West Nusa Tenggara, Indonesia. Journal of the Civil Engineering Forum, 7(3): 279−288. Petra Christian University. DOI: 10.22146/jcef.63417.

Rajaneesh A, Krishnapriya V, Sajinkumar K, et al. 2025. Predicting debris flow pathways using volume-based thresholds for effective risk assessment. Npj Natural Hazards, 2(1): 1. DOI: 10.1038/s44304-024-00055-2.

Rybchenko AA, Kadetova AV, Kozireva EA. 2018. Relation between basin morphometric features and dynamic characteristics of debris flows – a case study in Siberia, Russia. Journal of Mountain Science, 15(3): 618−630. DOI: 10.1007/s11629-017-4547-0.

Saaty TL. 2008. Decision making with the analytic hierarchy process. International Journal of Services Sciences, 1(1): 83−98. DOI: 10.1504/ijssci.2008.017590.

Salm B. 1993. Flow, flow transition and runout distances of flowing avalanches. Annals of Glaciology, 18: 221−226. DOI: 10.3189/s0260305500011551.

Sattar A, Haritashya UK, Kargel JS, et al. 2022. Transition of a small Himalayan glacier lake

outburst flood to a giant transborder flood and debris flow. Scientific Reports, 12(1): 12421. DOI：10.1038/s41598-022-16337-6.

Scheuner T, Schwab S, McArdell B. 2011. Application of a two-dimensional numerical model in risk and hazard assessment in Switzerland. Italian Journal of Engineering Geology and Environment, 993−1001. DOI：10.4408/IJEGE.2011-03.B-108.

Searle MP. 2011. Geological evolution of the Karakoram Ranges. Italian Journal of Geosciences, 130(2): 147−159. DOI：10.3301/ijg.2011.08.

Shafique M, van der Meijde M, Khan MA. 2016. A review of the 2005 Kashmir earthquake-induced landslides; from a remote sensing prospective. Journal of Asian Earth Sciences, 118: 68−80. DOI：10.1016/j.jseaes.2016.01.002.

Shah NA, Shafique M, Ishfaq M, et al. 2023. Integrated approach for landslide risk assessment using geoinformation tools and field data in Hindukush Mountain Ranges, Northern Pakistan. Sustainability, 15(4): 3102. DOI：10.3390/su15043102.

Shah NA, Shafique M, Owen LA, et al. 2025. Morphometric analysis of debris flow hazard and risk assessment in the mountain terrains of northern Pakistan using remote sensing and field data. Earth Science Informatics, 18(3): 295. DOI：10.1007/s12145-025-01807-y.

Shahzad L, Ali M, Sharif F, et al. 2024. Managing disasters in mountains: Challenges in the Era of Global Warming. Warming Mountains: Implications for Livelihood and Sustainability. Springer: 213−233. DOI：10.1007/978-3-031-62197-0_11.

Simoni A, Mammoliti M, Graf C. 2012. Performance Of 2D debris flow simulation model RAMMS. Annual International Conference on Geological and Earth Sciences GEOS. DOI：10.5176/2251-3361_geos12.59.

Tang C, Liu XL, Zhu J. 1993. The evaluation and application of risk degree for debris flow inundation on alluvial fans. Journal of Natural Disasters, 2(4): 79−84.

Tang Y, Guo Z, Wu L, et al. 2022. Assessing debris flow risk at a catchment scale for an economic decision based on the LiDAR DEM and numerical simulation. Frontiers in Earth Science, 10: 821735. DOI：10.3389/feart.2022.821735.

Turbessi L, Taboni B, Umili G, et al. 2025. Modeling debris flow events in the Rio Inferno Watershed (Italy) through UAV-based geomorphological survey and rainfall data analysis. Sensors, 25(7): 1980. DOI：10.3390/s25071980.

Ullah I, Shafique M, Khattak GA, et al. 2024. Debris flow simulations for hazard, vulnerability and risk assessment in the Karakorum mountain ranges, northern Pakistan. Remote Sensing Applications: Society and Environment, 36: 101389. DOI：10.1016/j.rsase.2024.101389.

Utley I, Hales T, Hussain E, et al. 2025. Transformations in exposure to debris flows in post-earthquake Sichuan, China. Natural Hazards and Earth System Sciences, 25(8): 2699−2716. DOI：10.5194/nhess-25-2699-2025.

Xiao H, Tang X, Zhang H. 2020. Risk assessment of debris flow in longchi area of dujiangyan based on GIS and AHP. IOP Conference Series: Earth and Environmental Science, IOP Publishing, 474(4): 042010. DOI：10.1088/1755-1315/474/4/042010.

Xiao Q, Wang S, He N, et al. 2024. Risk zoning method of potential sudden debris flow based on deep neural network. Water, 16(4): 518. DOI：10.3390/w16040518.

Yamanoshita M. 2019. IPCC special report on climate change and land: JSTOR.

Zhou W, Qiu H, Wang L, et al. 2022. Combining rainfall-induced shallow landslides and subsequent debris flows for hazard chain prediction. Catena, 213: 106199. DOI：10.1016/j.catena.2022.106199.

Zhou Y, Yue D, Liang G, et al. 2022. Risk assessment of debris flow in a mountain-basin area, western China. Remote Sensing, 14(12): 2942. DOI：10.3390/rs14122942.

Zou Q, Cui P, Chao Z, et al. 2016. Dynamic process-based risk assessment of debris flow on a local scale. Physical Geography, 37: 132−152. DOI：10.1080/02723646.2016.1169477.